

## Advances in Geostationary-Derived Longwave Fluxes for the CERES Synoptic (SYN1deg) Product

DAVID R. DOELLING

*NASA Langley Research Center, Hampton, Virginia*

MOGUO SUN, LE TRANG NGUYEN, MICHELE L. NORDEEN, CONOR O. HANEY, DENNIS F. KEYES,  
AND PAMELA E. MLYNCZAK

*Science Systems and Applications, Inc., Hampton, Virginia*

(Manuscript received 9 July 2015, in final form 20 November 2015)

### ABSTRACT

The Clouds and the Earth's Radiant Energy System (CERES) project has provided the climate community 15 years of globally observed top-of-the-atmosphere fluxes critical for climate and cloud feedback studies. To accurately monitor the earth's radiation budget, the CERES instrument footprint fluxes must be spatially and temporally averaged properly. The CERES synoptic 1° (SYN1deg) product incorporates derived fluxes from the geostationary satellites (GEOs) to account for the regional diurnal flux variations in between *Terra* and *Aqua* CERES measurements. The Edition 4 CERES reprocessing effort has provided the opportunity to reevaluate the derivation of longwave (LW) fluxes from GEO narrowband radiances by examining the improvements from incorporating 1-hourly versus 3-hourly GEO data, additional GEO infrared (IR) channels, and multichannel GEO cloud properties. The resultant GEO LW fluxes need to be consistent across the 16-satellite climate data record. To that end, the addition of the water vapor channel, available on all GEOs, was more effective than using a reanalysis dataset's column-weighted relative humidity combined with the window channel radiance. The benefit of the CERES LW angular directional model to derive fluxes was limited by the inconsistency of the GEO cloud retrievals. Greater success was found in the direct conversion of window and water vapor channel radiances into fluxes. Incorporating 1-hourly GEO fluxes had the greatest impact on improving the accuracy of high-temporal-resolution fluxes, and normalizing the GEO LW fluxes with CERES greatly reduced the monthly regional LW flux bias.

### 1. Introduction

The National Aeronautics and Space Administration's (NASA) Clouds and the Earth's Radiant Energy System (CERES) mission has currently provided the climate community a 15-yr record of observed top-of-the-atmosphere (TOA) fluxes (Wielicki et al. 1996). Accurate knowledge of the earth radiation budget is critical for cloud and climate feedback studies (Wielicki et al. 2013). The CERES-observed footprint fluxes must be spatially and temporally averaged to monitor the earth's global energy balance.

CERES instruments flown on board the *Terra*, *Aqua*, and *Suomi–National Polar-Orbiting Partnership* satellites

have been operational since February 2000, June 2002, and January 2012, respectively. These satellites were launched in sun-synchronous orbits with local equator crossing times (LECT) of 1030, 1330, and 1330 LT, respectively. All CERES Edition-3 instrument TOA radiances were radiometrically scaled to the *Terra* flight model (FM) 1 instrument (Loeb et al. 2012) to avoid temporal discontinuities in the flux record with the introduction of new CERES instruments. The CERES footprint radiances are converted into fluxes using scene-dependent angular directional models (ADMs) (Loeb et al. 2003, 2005) based on the CERES project's Moderate Resolution Imaging Spectroradiometer (MODIS) imager cloud retrievals (Minnis et al. 2011).

To estimate the daily mean flux, CERES uses two different approaches to account for the diurnal fluctuations of longwave (LW) regional fluxes in between the CERES measurements. The constant meteorology

---

*Corresponding author address:* David Doelling, NASA Langley Research Center, 21 Langley Blvd., MS 420, Hampton, VA 23681-2199.

E-mail: david.r.doelling@nasa.gov

approach, used in the CERES single-scanner footprint  $1^{\circ}$  (SSF1deg) product, assumes that the cloud conditions at the time of measurement represent the conditions throughout the day. Over ocean, the daily LW flux is then based on linear interpolation between the daytime and nighttime CERES measurements. Over land, a half-sine shape centered at noon with a constant nighttime flux describes the hourly LW flux to account for the daytime solar heating (Doelling et al. 2013). These algorithms are similar to those employed by the Earth Radiation Budget Experiment (ERBE) (Young et al. 1998). The second approach incorporates broadband fluxes derived from contiguous geostationary satellite (GEO) imager radiances between  $60^{\circ}\text{N}$  and  $60^{\circ}\text{S}$ . The diurnally complete synoptic  $1^{\circ}$  (SYN1deg) product uses this approach, combining *Terra*, *Aqua*, and GEO observations. This product also contains the computed in-atmosphere and surface fluxes based on both the MODIS and GEO imager-derived CERES cloud retrievals (Rutan et al. 2015). The CERES product processing flowchart can be found at online (at [http://ceres.larc.nasa.gov/science\\_information.php?page=system-flow](http://ceres.larc.nasa.gov/science_information.php?page=system-flow)), and the CERES GEO temporal interpolation flowchart is available in Doelling et al. (2013, their Fig. 2).

The monthly regional shortwave (SW) and LW flux differences between the two approaches can be as great as  $25$  and  $8\text{ W m}^{-2}$ , respectively, over maritime stratus and afternoon land convective regions. However, the global mean flux differences are within  $\sim 1\text{ W m}^{-2}$  for both SW and LW (Doelling et al. 2013). The GEO fluxes are used to account for regional diurnal cycles. However, because of the varying quality of the GEO fluxes and clouds from 16 satellites since 2000, GEO artifacts may introduce spurious long-term regional trends in the SYN1deg TOA flux record. Therefore, the SYN1deg product is not suited to determine regional long-term trends, unlike the SSF1deg product, which relies only on the CERES instrument calibration for stability. Taylor and Loeb (2013) reported that diurnal-cycle fluctuations are small contributors to the long-term regional trends.

To prepare for the CERES Edition 4 products, the CERES instrument calibration, MODIS-derived cloud retrievals, ADMs, and GEO clouds and fluxes have been reevaluated in order to improve the accuracy of the observed TOA and computed surface fluxes. The Edition 4 effort also presented the opportunity to improve the GEO-derived LW broadband fluxes over those used in Edition 3 by utilizing multiple infrared (IR) GEO channels, multichannel GEO imager-based cloud properties, and hourly GEO images. There are four overall components to derive the GEO LW fluxes: 1) the GEO IR channel calibration, 2) the GEO LW narrowband

(NB) to broadband (BB) algorithm, 3) the LW flux temporal interpolation, and 4) the normalization of the GEO-derived LW fluxes to the CERES-observed fluxes to remove any residual GEO-derived LW flux biases.

Three GEO NB-to-BB algorithms are considered: 1) the column-weighted relative humidity approach (colRH), which utilizes the GEO window channel radiance and the RH from an assimilated model to estimate the LW flux; 2) the radiance-based algorithm (RBA), which directly converts the GEO window and water vapor channel radiances to LW flux, binned according to radiance and other observed conditions; and 3) the scene-based algorithm (SBA), which converts the GEO window and water vapor channel radiances to LW radiance, binned according to the CERES ADM scene type, and then uses the CERES ADM to convert the radiance to LW flux. This algorithm also takes advantage of the multichannel GEO imager cloud properties.

Two LW temporal interpolation approaches are evaluated: 1) the 3-h GEO approach that utilizes 3-hourly GEO-derived LW fluxes and temporally interpolates the fluxes throughout the day to compute the daily mean LW flux; and 2) the 1-h GEO approach, which simply averages the hourly GEO-derived fluxes to compute the daily mean LW flux.

Two GEO-derived LW normalization routines are analyzed: 1) instantaneous normalization, which updates the regional scaling factors whenever the GEO and CERES LW fluxes can be matched within one hour; and 2) regional normalization, which applies monthly regional scaling factors based on the linear regression of GEO and CERES LW matched flux pairs within a moving  $5^{\circ}$  latitude by  $5^{\circ}$  longitude domain.

The current CERES Edition 3 processing uses the colRH algorithm, 3-h GEO sampling, and instantaneous normalization. The new approaches are expected to improve upon the current Edition 3 approach, but they need to be evaluated against it. The relative contribution of each component also needs to be assessed.

This study is organized by first describing the GEO IR radiances and their calibration with MODIS in section 2. Section 3 outlines the GEO LW NB radiance to BB flux approaches. Section 4 describes the LW temporal interpolation and normalization with CERES fluxes. Section 5 validates the GEO LW flux approaches with CERES-observed fluxes. The diurnal fluxes from the various GEO LW flux approaches are compared against hourly Geostationary Earth Radiation Budget (GERB)-observed LW fluxes in section 6. The conclusions are found in section 7.

TABLE 1. Beginning (beg) and ending (end) scan times (minutes, seconds of the hour) for the GEOs used over the CERES record. All full disk (FD) scans provide complete spatial coverage between 60°N and 60°S. The GOES satellites scan a full disk every third hour beginning with 0 UTC. For the remaining hours, the Northern Hemisphere (NH) and Southern Hemisphere (SH) scans provide continuous coverage between 60°N and 50°S. *GMS-5* scans an hourly sequence of NH, NH, FD, NH, FD, FD, every 6 h. The *GMS-5* NH scan domain encompasses 60°N–12°S.

Satellite	Full disk		NH		SH	
	Beg (min, s)	End (min, s)	Beg (min, s)	End (min, s)	Beg (min, s)	End (min, s)
<i>Met-7</i> at 0°	30, 00	55, 00				
<i>Met-8, -9, -10</i>	00, 00	12, 00				
<i>Met-5, -7</i> at 60°E	30, 00	55, 00				
<i>GMS-5</i>	32, 00	58, 00	32, 00	48, 00		
<i>GOES-9</i>	25, 00	51, 06				
<i>MTSAT-1R, -2</i>	32, 00	58, 00				
<i>GOES-10, -11, -15</i>	00, 00	26, 06	00, 00	10, 15	22, 00	29, 00
<i>GOES-8, -12, -13</i>	45, 00	11, 06	45, 00	59, 15	09, 00	13, 49

## 2. GEO data and calibration

### a. GEO imager radiance and clouds

One-hourly GEO images are obtained from Man Computer Interactive Data Access System (McIDAS) (Lazzara et al. 1999), which provides a consistent data format across GEO platforms. The GEO nominal 1-km visible and 4-km IR pixel resolution images are subsampled into 8-km pixel resolution images. At any given time during the CERES record, five GEO satellites provide contiguous coverage between 60°N and 60°S. Sixteen satellites from the Geostationary Operational Environmental Satellite (GOES), Geostationary Meteorological Satellite (GMS), Meteorological Satellite [Meteosat (Met)], and Multifunctional Transport Satellite (MTSAT) series comprise the CERES GEO record and are listed in Table 1 along with the times they begin and end their hourly scans. All GEOs during the CERES record scan at least hourly; however, the GEOs do not scan at the same time within the hour. Also, the Met satellites scan from the south to north, whereas all other satellites scan in the opposite direction.

Figure 1 displays the CERES GEO constellation from 2000 to 2014 by the GEO subsatellite longitude position. The GEO satellites are color-coded by IR channel features. The first-generation satellites (green) contain two IR channels, a 10.8-μm window (WIN) channel and a 6.7-μm water vapor (WV) channel. The earlier second-generation GOES-like satellites (dark blue) have added 3.9- and 12-μm channels. The later GOES satellites (cyan) have replaced the 12-μm channel with the 13.3-μm channel. The second-generation Met satellites (red) have all the previously mentioned IR channels along with 7.4-, 8.7-, and 9.7-μm channels. Outside of the Indian Ocean domain (60°E), all of the GEOs operational after 2004 have at least five channels, one visible and four IR (see Fig. 1). The third-generation *Himawari-8*

Advanced Himawari Imager and GOES Advanced Baseline Imager (Schmit et al. 2005) are expected to be operational in 2015 and 2017, respectively, and will include all of the Met second-generation IR channels and additional 6.25- and 10.3-μm channels.

The Edition 3 CERES GEO cloud retrievals are based on the visible and WIN channel radiances, which are used in the Layered Bispectral Threshold Model (Minnis et al. 1994). For Edition 4, the CERES GEO cloud detection and cloud property retrievals will take advantage of the available IR channels, incorporating the 3.9-μm and either the 12- or 13.3-μm channels to more accurately estimate the cloud particle size, optical depth, and height. The more MODIS-like GEO-retrieved clouds and the additional IR channels are expected to improve the accuracy of the GEO LW NB-to-BB fluxes. The Edition 3 GEO clouds used a static cloud particle size and assumed a nighttime emissivity of

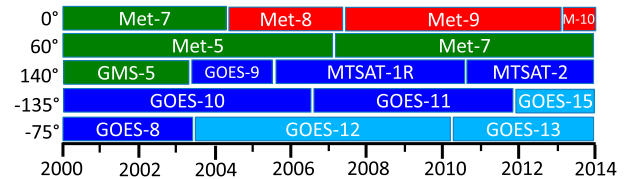


FIG. 1. Geostationary satellite timelines used in CERES processing, listed by subsatellite longitude position. GEOs with 6.7- and 10.8-μm channels are in green. GEOs with 3.9-, 6.7-, 10.8-, and 12-μm channels are in dark blue. GEOs that have replaced the 12-μm channel with a 13.3-μm channel are in cyan. GEOs with 3.9-, 6.7-, 7.4-, 8.7-, 9.7-, 10.8-, 12-, and 13.3-μm channels are in red. The aim of this chart is to broadly display the geostationary timelines. This chart does not display the *GOES-14* operational periods 24 Sep–17 Oct 2012 and 23 May–9 June 2013 due to a *GOES-13* instrument anomaly. Neither is the MTSAT annual ground maintenance time period displayed, where the operational MTSAT is replaced with the standby MTSAT for a few weeks near the end of the year. The remaining operational satellite outages, which typically persist less than a week, are also not displayed.

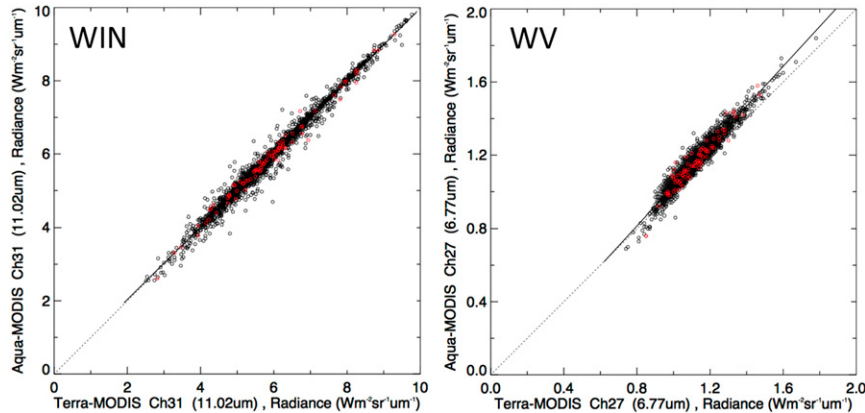


FIG. 2. Scatterplot of the *Terra* and *Aqua* MODIS nadir (red points) and off-nadir (black points) radiance pairs for June 2010 for the (left) WIN channel and (right) WV channel. The associated regression line (solid) and perfect agreement line (dotted) are also shown.

unity, which had the effect of placing semitransparent clouds too low in the atmosphere (Minnis et al. 1994).

#### b. GEO imager radiance calibration with *Aqua MODIS*

The Edition 3 GEO IR channel brightness temperatures (BTs) were referenced to the *Terra* MODIS calibration to ensure consistency across GEO platforms. All of the GEO channel BTs were adjusted to the corresponding MODIS-equivalent IR temperatures, without accounting for spectral band response differences, to facilitate the GEO cloud retrieval algorithm. Since the *Terra* and *Aqua* MODIS spectral response functions are nearly identical, any IR radiance difference between *Terra* and *Aqua* is due to the onboard calibration. *Terra* and *Aqua* WIN channel and WV channel simultaneous nadir overpass daytime (within 15 min) radiance pairs for June 2010 are plotted in Fig. 2 following the visible approach in Minnis et al. (2008) and Doelling et al. (2015). *Terra* and *Aqua* MODIS pixel radiances are averaged within a 25-km radius of the *Terra* and *Aqua* orbital intersect. Off-nadir pairs located along the equal view zenith angle (VZA) trajectory between the two satellites are also plotted to increase the sampling and dynamic range. The WIN channel radiances are similar, having a slope of 0.9925 with an RMS error of 2.7% and an overall bias of 0.2%. For WV the radiance pairs are not distributed linearly. This case has a slope of 1.0890 with an RMS error of 4.9% and an overall bias of 3.4%. It was recently documented that the *Terra* MODIS WV channel is affected by a crossband signal leak (Sohn et al. 2008, 2010; Sun et al. 2011). Therefore, the Edition 4 IR channels will be calibrated against *Aqua* MODIS.

To convert the GEO IR channel BTs to corresponding MODIS-equivalent IR channel BTs, the GEO IR channel BTs are adjusted monthly using linear regressions of 50-km gridded GEO and MODIS IR channel coincident, collocated, and VZA-matched temperature pairs (Doelling et al. 2013) as shown in the top row of Fig. 3. The GEO minus *Aqua* MODIS monthly temperature biases are shown for *Met-9* and *Met-7* in the middle row of Fig. 3. The relative calibration effects of a *Met-9* deicing event in early 2008 can be seen in both the WIN and WV channels. For *Met-7*, a drift of the WIN temperature in time is observed when compared with MODIS.

The Global Space-Based Intercalibration System (GSICS) (Goldberg et al. 2011) IR calibrations are now available for GEOS beginning in 2007. However, they are not used here because they provide the true IR BTs, whereas GEO MODIS-equivalent IR BTs are required for the GEO LW NB-to-BB coefficients (section 3). The GSICS GEO IR calibration is based on convolving the hyperspectral Infrared Atmospheric Sounding Interferometer (IASI) radiances with the sensor spectral response function (Fig. 4) (Hewison et al. 2013). The bottom row of Fig. 3 displays the GEO minus GSICS-corrected GEO monthly temperature biases with respect to IASI. For the *Met-9* WIN and WV channels, the BT difference is minimal with respect to the GSICS calibration. However, the *Met-9* BT difference with respect to MODIS is greater (Fig. 3 middle row), indicating that the MODIS and GEO BT difference is mostly spectral, especially for the WV. The GEO MODIS-equivalent IR temperature may also include MODIS IR calibration anomalies, given that the *Aqua* MODIS WIN and WV Collection 5 BTs are within  $0.2 \pm 0.2$  K and  $-0.6 \pm 0.3$  K, respectively,

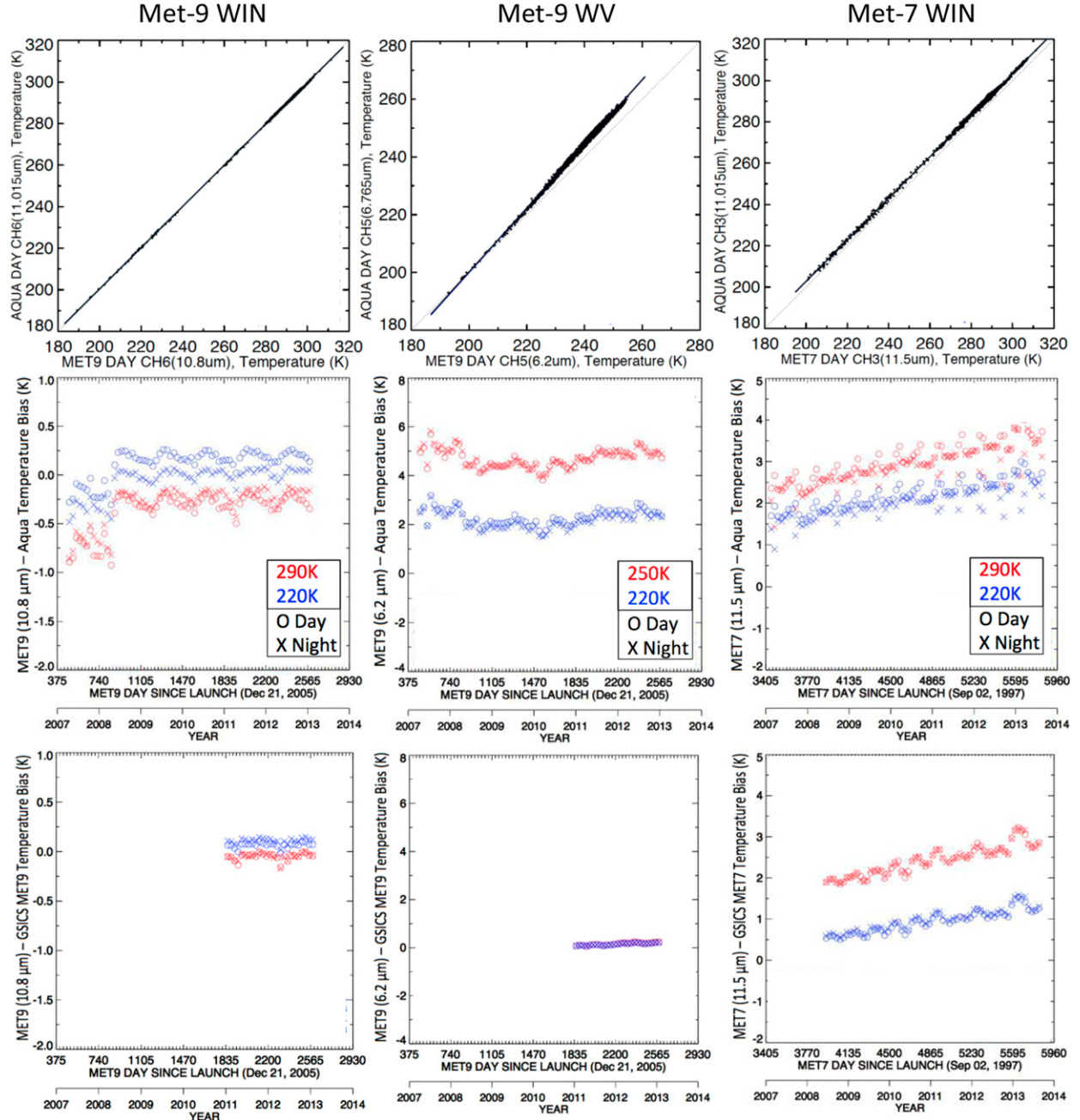


FIG. 3. (top row) Scatterplot of temperature pairs for the (left) *Met-9 WIN*, (middle) *Met-9 WV*, and (right) *Met-7 WIN* channel and corresponding *Aqua* MODIS channel for June 2012. The associated regression line (black) is also shown. (middle row) The 2007–13 monthly temperature biases at 290 (red) and 220 K (black) for day (o) and night (x) for *Met-9 WIN*, *Met-9 WV*, and *Met-7 WIN* minus *Aqua* MODIS. For *Met-9 WV* the bias at 290 K is replaced with the bias at 250 K. (bottom row) As in middle row, except for GEO minus GSICS-corrected GEO monthly temperature biases. The GSICS correction is only available beginning in 2011 for *Met-9* and in 2008 for *Met-7*.

with respect to IASI (Li et al. 2013). The seasonal variability of the GEO BT difference with respect to MODIS is also due to the spectral difference. The *Met-7* WV BT difference drift is due to calibration. After applying the GSICS calibration to all GEO satellites, it

was found that the GEO WIN and WV BT biases were within 0.4 K, similar to the results in Hewison et al. (2013), except for *Met-7*. This suggests that for most satellites, the GEO minus MODIS IR BT differences are due to spectral band differences.

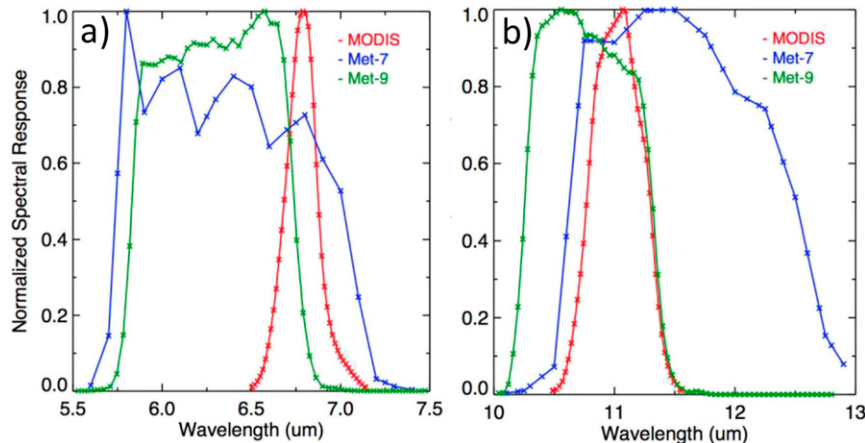


FIG. 4. The normalized spectral response functions for *Aqua* MODIS, Met-7, and Met-9 for the (a) WV and (b) WIN channels.

### 3. GEO LW narrowband radiance to broadband flux

The estimation of LW fluxes from GEO IR imager radiances has been an ongoing effort since the first GEO satellites. Gube (1982) converted the Met WIN and WV imager radiances into LW fluxes using third-order polynomial coefficients stratified by VZA based on radiative transfer (RT) model radiances from a database of atmospheric profiles. Schmetz and Liu (1988) replaced the stratification by VZA with a limb-darkening function and remarked that the addition of the WV channel reduced the LW RMS error by half. Cheruy et al. (1991) also used polynomial regressions based on an RT model of the Met WIN and WV channel radiances, compared coincident Met and ERBE LW fluxes, and commented that the two channels nearly accounted for all of the OLR variance. Dewitte and Clerbaux (1999) observed that including all of the Met second-generation IR channels in the polynomial regression from an RT model reduced the LW RMS error by 40% over the results using only the Met first-generation WIN and WV channels. Viollier et al. (2004) used coincident Met-5 WIN and WV radiances and Scanner for Radiation Budget (ScaRaB) LW measurements to derive NB-to-BB polynomial coefficients, with results similar to Cheruy et al. (1991). They also compared the Met LW fluxes with coincident CERES fluxes and found that the bias was less than  $1 \text{ W m}^{-2}$ . Singh et al. (2007) studied the Kalpana WIN and WV channels with a genetic algorithm using a variety of polynomial equations and concluded that the best regression had a simple linear WIN and WV term.

Lee et al. (2004) derived GOES WV channel and 12- $\mu\text{m}$  imager channel linear regression coefficients stratified by VZA to estimate the LW flux and noted a 20%

reduction in the RMS error when using the GOES WV, WIN, and 13.3- $\mu\text{m}$  channels instead, since the 13.3- $\mu\text{m}$  channel provides lower-tropospheric temperature information. Lee et al. (2008) compared the Met second-generation 7.3-, 10.8-, and 13.3- $\mu\text{m}$  channel-based LW fluxes and the 6.2-, 7.3-, 8.7-, and 13.3- $\mu\text{m}$  channel-based LW fluxes with CERES and noted that the RMS error was reduced by  $4.5\text{--}4 \text{ W m}^{-2}$ , or 12%, by adding more channels. Further reduction was achieved by adding the 10.8- $\mu\text{m}$  channel radiances and the square and cube of the 13.3- $\mu\text{m}$  channel radiances using stagewise and nonlinear coefficients. Doelling et al. (2003) found for a single-channel IR algorithm that the *GOES-8* 12- $\mu\text{m}$  channel was more effective than the 10.8- $\mu\text{m}$  channel compared with CERES LW fluxes, but after adding the WV channel there was little RMS error difference between the two.

The preferable method to obtain the LW NB-to-BB regression coefficients is to utilize GEO and CERES coincident, collocated, and coangled measurements over all scene types. Since each GEO has its unique IR spectral response function, each GEO will require its own set of coefficients. Coincident ray-matched locations from the GEO and sun-synchronous satellites (i.e., *Terra*, *Aqua*) are not well distributed across the GEO image, limiting the sampling of different surface, atmospheric, and cloud conditions. Therefore, as with the Edition 3 approach, the monthly LW NB-to-BB coefficients will be based on the perfectly coincident ray-matched MODIS IR channel radiances and CERES LW fluxes found in the CERES SSF product between  $60^\circ\text{N}$  and  $60^\circ\text{S}$ . The coefficients will then be applied to the GEO IR radiances after they have been converted to MODIS-equivalent IR radiances. This approach may not capture the entire LW dynamic range observed by

the GEO measurements, such as noontime desert and late afternoon land convective conditions that are not observed by either *Terra* or *Aqua*. The fluxes from these extreme conditions can be validated geographically against hourly GERB fluxes (see section 6).

Historical studies indicate that most of the LW information is contained in the WIN and WV channels, with diminishing returns from additional IR channels. The WIN and WV channels are found on all GEOS during the CERES record, thereby providing the most consistent LW fluxes across all GEOS. Varying the number of GEO IR channels utilized may cause LW flux discontinuities across satellite boundaries. Although it is possible to compute coefficients using all available GEO IR channels associated with a similar MODIS channel, it presents an operational challenge. Because of the inferior quality of GEO images, which may contain spurious pixel-level radiances, the addition of more IR channels increases the risk of erroneous LW fluxes resulting from the spurious radiances. The CERES Edition 3 product GEO data has not been quality controlled, and corrupted scan lines are embedded in the imagery. Since 2011, the GEO visible and WIN imagery are visually inspected, and corrupted scan lines are removed. CERES Edition 4 GEO data will be quality controlled with a combination of automated and human visualization efforts, since the volume of data will be much greater.

#### a. colRH approach

The CERES Edition 3 uses a column-weighted relative humidity (colRH) approach that is described in detail in [Doelling et al. \(2013\)](#) and summarized here. The GEO WIN flux is computed from the WIN radiance using a limb-darkening factor ( $\gamma$ ) based on VZA following Eq. (1). The WIN flux is then converted to LW flux using a quadratic function with a column-weighted relative humidity term to estimate the water vapor absorption contribution using Eq. (2) ([Minnis et al. 1991; Young et al. 1998](#)):

$$\text{WIN}_{\text{flux}} = 6.18\gamma(\text{VZA})\text{WIN}_{\text{rad}} \quad (1)$$

$$\begin{aligned} \text{LW}_{\text{flux}} &= a_0 + a_1 \text{WIN}_{\text{flux}} + a_2 \text{WIN}_{\text{flux}}^2 \\ &\quad + a_3 \text{WIN}_{\text{flux}} \ln(\text{colRH}). \end{aligned} \quad (2)$$

CERES uses atmospheric profiles from the Global Modeling and Assimilation Office (GMAO) Goddard Earth Observing System GEOS-5.4.1 assimilation dataset ([Rienecker et al. 2011](#)) to obtain column-weighted relative humidity. The monthly coefficients are derived empirically from the perfectly matched MODIS WIN channel radiances and CERES LW fluxes on the CERES SSF product. Global ocean and land coefficients are

derived separately. The coefficients are found not to vary in time. Only a single set of monthly coefficients is used for the entire record.

#### b. Radiance-based approach

The radiance-based algorithm (RBA) converts the WIN and WV radiances to LW fluxes by binning according to WIN radiance, VZA, day/night, precipitable water (PW) from the GEOS 5.4.1 dataset, clear/cloudy conditions from the CERES GEO four-channel cloud retrievals, and surface type to remove the nonlinear spectral, limb-darkening, and regional dependencies of the GEO LW flux. There are 35 VZA bins of  $2^\circ$  from  $0^\circ$  to  $70^\circ$ , six WIN radiance bins of  $2 \text{ W m}^{-2} \text{ sr}^{-1} \mu\text{m}^{-1}$  each, and four PW bins. There are six surface types grouped by International Geosphere–Biosphere Programme (IGBP) type that correspond to the surface albedo brightness and are identified as ocean, dark and bright land, dark and bright desert, and snow; all are static except for snow ([Loeb et al. 2005](#)). For each bin the LW NB-to-BB flux multilinear regression coefficients are computed using Eq. (3):

$$\text{LW}_{\text{flux}} = a_0 + a_1 \text{WIN}_{\text{rad}} + a_2 \text{WV}_{\text{rad}}. \quad (3)$$

The coefficients are computed monthly from the matched MODIS WIN channel radiances and CERES SSF LW fluxes.

#### c. Scene-based approach

The SBA increases the number of scene conditions by taking advantage of the improved four-channel GEO cloud properties and utilizing the CERES LW ADM to convert radiances into fluxes. This algorithm uses the same scene binning as the CERES LW ADM to convert the GEO IR radiances into BB radiances. It incorporates six surface types, seven VZA, three PW, and day/night bins, as well as five cloud amount, five cloud emissivity, and six lapse rate bins based on the GEOS 5.4.1 dataset and CERES GEO four-channel cloud retrievals. The lapse rate is defined as the surface minus cloud-top temperature difference, or in the case of clear sky, the surface minus 300-hPa temperature. For each bin the LW NB-to-BB coefficients are computed using Eq. (4):

$$\text{LW}_{\text{rad}} = b_0 + b_1 \text{WIN}_{\text{rad}} + b_2 \text{WV}_{\text{rad}} \quad (4)$$

The coefficients are computed monthly from the matched MODIS WIN channel radiances and CERES SSF LW radiances. The CERES LW ADM is then used to convert the LW radiance to a flux.

Essentially, the RBA assumes that the spectral dependency is radiance based and that various cloud conditions with the same WIN and WV radiances will

have similar coefficients, whereas the SBA allows cloud conditions with the same radiances to have unique coefficients.

#### 4. LW temporal interpolation and normalization

##### a. LW temporal interpolation

The CERES or GEO LW measurements are assigned into 24 hourly increments, or hourboxes, per day. The hourbox range is between UTC whole hours, that is, 0–1 UTC, 1–2 UTC, etc. This is a departure from the ERBE temporal averaging where the hourboxes were defined in local time. When both a CERES measurement and a GEO LW measurement are within the same hourbox, the CERES observation takes precedence. Then, the linear interpolation between observed hourboxes fills the remaining unsampled hourboxes. The SYN1deg Edition 3 product incorporates 3-hourly GEO data. Typically within 45°N–45°S, there are two *Aqua* CERES, two *Terra* CERES, and eight 3-hourly GEO daily measurements; the remaining 12 h are composed of interpolated LW fluxes. For the SYN1deg Edition 4 product, 1-hourly GEO imagery will be utilized. This will eliminate the need for temporal interpolation unless there is a data gap. Therefore, the addition of hourly GEO fluxes and clouds is expected to increase the accuracy of the TOA LW flux, as well as the associated computed surface and in-atmosphere LW fluxes.

##### b. Instantaneous normalization

For the SYN1deg Edition 3 product, the residual GEO OLR biases are removed by instantaneously scaling the GEO-derived LW flux to the observed CERES OLR. This is performed whenever a CERES and GEO measurement are contained within the same hourbox. The scaling factor is interpolated between CERES measurement hourboxes and applied to all GEO and interpolated LW hourbox fluxes. This ensures that the monthly regional GEO-derived LW fluxes are on the same radiometric scale as the CERES fluxes. The drawback of instantaneous normalization is that the normalization factor not only contains the LW NB-to-BB flux bias but also the GEO and CERES time difference matching error, which can be as large as 59 min. This may result in unrealistic normalized LW fluxes, especially when warm clear-sky and cold high thick cloud conditions are observed in the same hourbox.

##### c. Regional normalization

GEO LW to CERES flux normalization in Edition 4 will incorporate the regional normalization algorithm

utilized for Edition 3 SW fluxes. This technique has been effective in removing residual biases, which are manifested regionally (Doelling et al. 2013). Regional GEO and CERES LW flux pairs coincident within 30 min from a moving 5° latitude by 5° longitude domain are regressed monthly to compute a monthly slope and offset for each region. Only regions with the same surface type within the same GEO domain are used to derive the normalization coefficients. Any LW flux difference within the hourbox due to changing meteorological conditions will be considered as noise along the linear regression line, as opposed to the instantaneous normalization, which would give an unrealistic normalization factor in this case.

#### 5. Validation with CERES fluxes

The objective of this section is to validate the SBA, which takes advantage of the MODIS-like four-channel GEO cloud properties, the RBA, which strives for consistency between GEO WIN and WV channels, and the Edition 3 colRH baseline LW flux approaches. *Terra* CERES LW observed fluxes are used as truth to validate the GEO-derived LW fluxes, where the LW NB-to-BB coefficients are computed from the *Aqua* SSF product's MODIS and CERES measurements and where the GEO fluxes are regionally normalized to the *Aqua* CERES fluxes. No *Terra* measurements are used to derive the GEO fluxes; they are used only to validate. For CERES Edition 3, the *Terra* instrument calibration was radiometrically scaled to the *Aqua* instrument calibration, implying that any *Terra* CERES and GEO LW flux difference is due to the GEO LW flux algorithm. The *Terra* (1030 LECT) and *Aqua* (1330 LECT) local crossing time difference is symmetric about both local noon and midnight. The time difference between the two satellites' orbits varies by 2 h at 60°N, 3 h at the equator, and 4 h at 60°S. Using a 30-min window to match the GEO and *Terra* CERES measurements ensures that all regions in the GEO domain have two measurements a day for validation.

##### a. LW approaches without normalization

Figure 5 displays the GEO dataset minus *Terra* CERES coincident (within 30 min) LW mean regional flux biases for January 2010. Figure 6 displays the corresponding regional RMS errors. The colRH\_no-norm (without normalization) approach has large regional biases over maritime stratus, Northern Hemisphere snow, the tropical western Pacific, and the South Pacific convergence zone. The large colRH\_no-norm regional biases and RMS errors near the poles suggest that the limb-darkening factor [see Eq. (1)] is inadequate for large

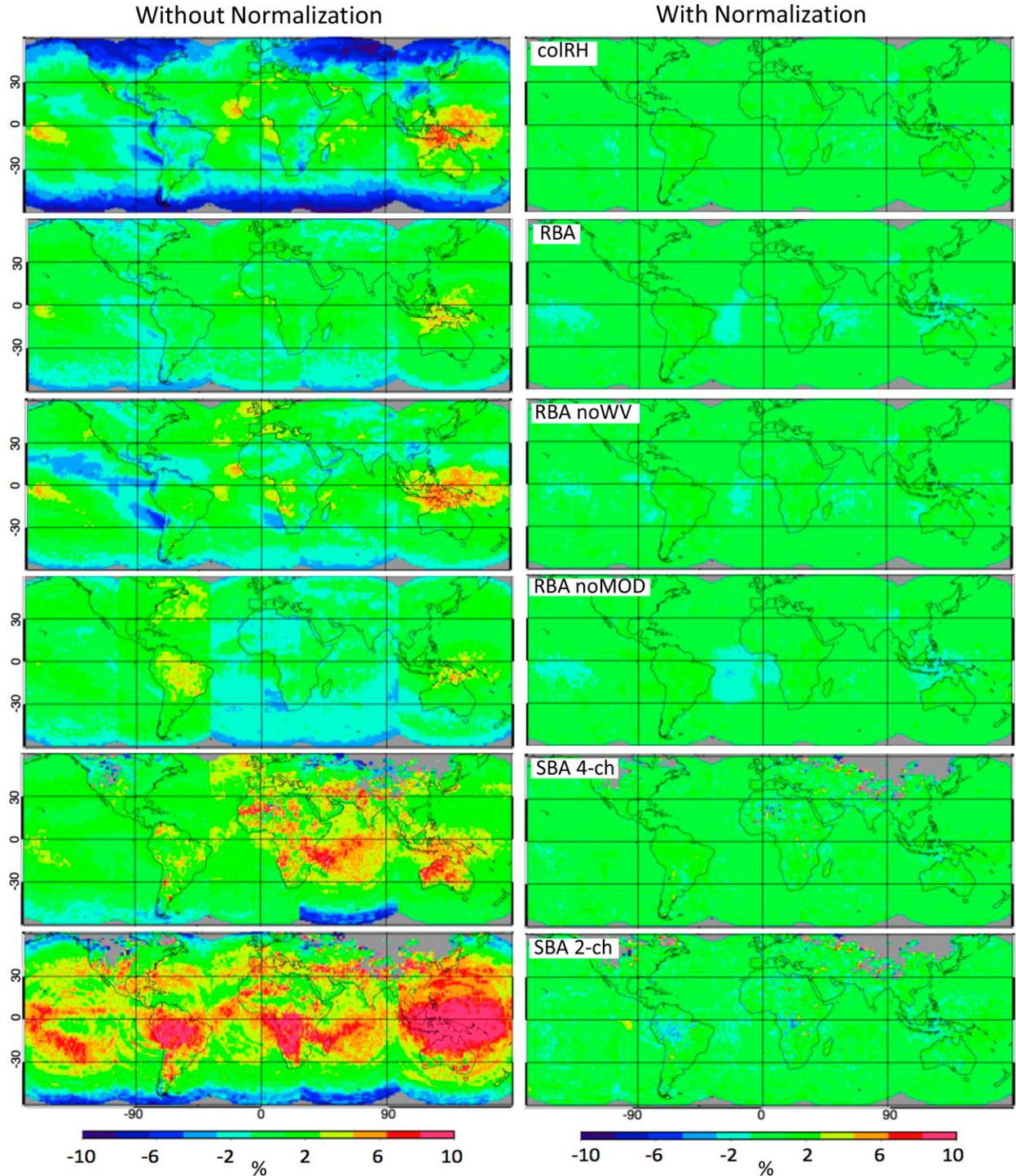


FIG. 5. The January 2010 1-h GEO LW flux dataset minus *Terra* CERES LW regional flux bias (%) (left) without normalization and (right) with *Aqua* regional normalization. (from top to bottom) The datasets are from the colRH approach, RBA, RBA without the WV channel, RBA without MODIS IR adjustment, SBA, and SBA with two-channel clouds.

GEO VZA conditions. The RBA\_no-norm regional biases and RMS errors occur over the same locations as those of the colRH\_no-norm but with a much smaller magnitude.

The SBA\_4ch\_no-norm (based on four-channel clouds but includes the Met-7 two-channel clouds) has smaller biases over the two GOES domains, which cover the Western Hemisphere, than the colRH\_no-norm

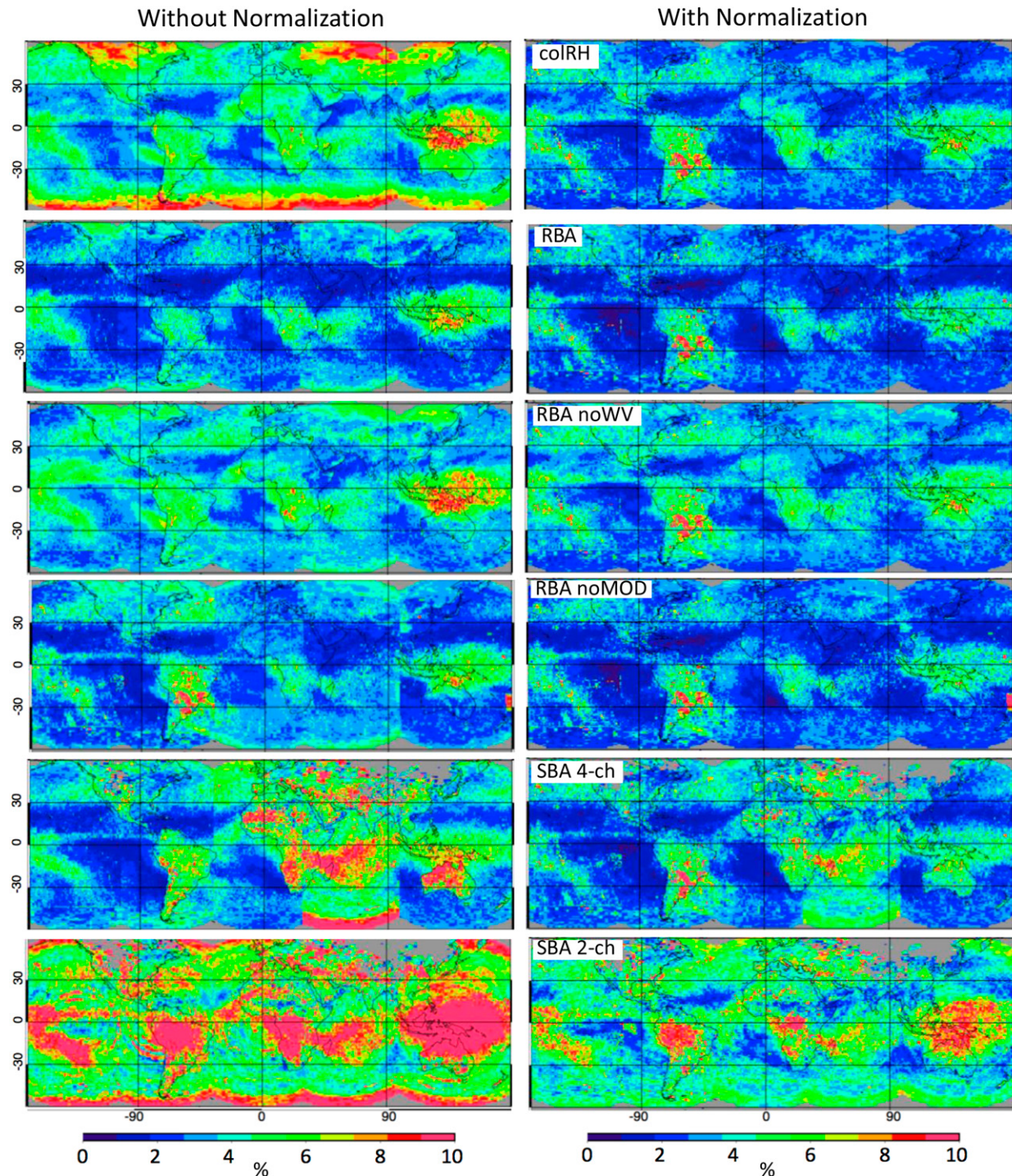


FIG. 6. As in Fig. 5, but for LW RMS error (%).

approach has (see Fig. 5). The cloud retrievals from *Met-9* ( $0^{\circ}$ E) and *MTSAT-1R* ( $140^{\circ}$ E) are also based on four channels, similar to GOES; however, *Met-7* over the Indian Ocean relies on two-channel cloud retrievals. The SBA\_4ch\_no-norm depends on consistent

MODIS and GEO cloud retrievals for proper scene identification to select the appropriate NB-to-BB coefficients and ADM. The SBA\_4ch\_no-norm seems to perform well over ocean; however, the biases over land are greater than for either the colRH\_no-norm or the

TABLE 2. The January 2010 LW flux dataset minus *Terra* CERES LW regional flux bias, standard deviation of the regional bias, and instantaneous RMS error using hourly GEO observations. For colRH, RBA, RBA\_noWV, RBA\_noMOD, SBA with four-channel clouds (SBA\_4ch), and SBA with two-channel clouds (SBA\_2ch) without normalization (no-norm) and with *Aqua* regional normalization (norm) datasets.

1-h GEO dataset	Std dev of regional bias (%)					
	Bias: GEO – CERES (%)		No-norm		RMS error (%)	
	No-norm	Norm	No-norm	Norm	No-norm	Norm
colRH	-0.74	0.15	2.39	0.52	3.83	2.57
RBA	0.24	0.08	1.17	0.58	2.62	2.28
RBA_NoWV	0.60	0.12	1.66	0.59	3.25	2.81
RBA_NoMOD	0.05	0.09	1.31	0.64	2.70	2.34
SBA_4ch	1.38	0.08	1.89	0.58	3.57	2.94
SBA_2ch	2.61	0.16	3.26	1.05	5.68	3.93

RBA\_no\_norm. For the SBA\_2ch\_no-norm (based on two-channel clouds), large regional biases and RMS errors seem to manifest themselves in circular VZA patterns, centered on the individual GEO domains. The SBA\_4ch\_no-norm and the SBA\_2ch\_no-norm gray regions over Northern Hemisphere land are covered by snow, where the GEO cloud retrievals are considered unreliable. The snow-covered regions rely on temporally interpolated MODIS cloud properties because no systematic diurnal variations in cloud conditions are expected over snow.

Table 2 shows that the RBA\_no-norm has reduced the absolute bias, standard deviation of the regional biases, and RMS error by 66%, 50%, and 30%, respectively, when compared with the colRH\_no-norm approach. The SBA\_2ch\_no-norm has a 250%, 35%, and 48% greater bias, regional standard deviation, and RMS error, respectively, than the colRH\_no-norm approach. The SBA\_4ch\_no\_norm, which includes the two-channel GEO domain, shows an improvement over the colRH\_no-norm approach, but it is inferior to the RBA\_no\_norm. The SBA\_4ch\_no\_norm is only successful if the MODIS clouds, which stratified the NB-to-BB coefficients, are consistent with the GEO clouds, which are used to apply the coefficients and the ADM.

#### b. LW approaches with regional normalization

Operationally, all approaches will normalize the GEO-derived fluxes with CERES fluxes. As intended, regional normalization has removed the regional bias regardless of approach (Fig. 5). The RMS errors of the various approaches in descending order are as follows: SBA\_2ch\_norm (with regional normalization), SBA\_4ch\_norm, colRH\_norm, and RBA\_norm (Table 2).

Because the SBA\_4ch\_norm has inconsistent GEO-dependent RMS errors (Fig. 6) and the colRH\_norm approach outperforms the SBA\_4ch\_norm, no further validation of the SBA is performed. It will be worthwhile to reevaluate the SBA LW fluxes using the improved future third-generation GEO cloud properties as they become available.

To determine the contribution of RBA components, the RBA is run for two more cases: 1) without the MODIS-equivalent IR calibration adjustment [see noMOD in Table 2 and Figs. 5 and 6] and 2) without the WV channel (noWV) by linearly regressing only the WIN channel [third term of Eq. (3)]. Without normalization there is only a slight advantage of the MODIS IR adjustment in reducing the regional bias and RMS error, and this advantage is diminished with normalization (Table 2). Therefore, the MODIS IR calibration is not crucial for consistent RBA normalized LW fluxes. Including the WV channel in the RBA has reduced the RMS error by ~20% in both normalized and unnormalized cases when compared with the RBA\_noWV approach (Table 2). With normalization the colRH\_norm approach has an RMS error of 10% greater than the RBA\_norm that includes the WV channel. This implies that the observed WV in the RBA is more effective than the assimilated WV profile in the colRH approach in predicting LW fluxes.

The VZA, PW, and radiance binning and the addition of the WV channel have improved the RBA over the colRH approach. The RBA was tested using LW NB-to-BB coefficients from three Januaries during 2002, 2003, and 2004, and with four seasonal months during 2003; the statistics were nearly identical to the statistics in Table 2, which used coefficients from January 2010. Like the colRH approach, the RBA coefficients seem to be stable in time. The CERES *Terra*-only time period will use 2002, 2003, and 2004 *Aqua* MODIS monthly climatology coefficients.

#### c. One-hour and three-hour GEO

To obtain 3-hourly GEO colRH and RBA datasets, the procedure is modified to incorporate only the full-disk (FD) GEO imagery, available at 0, 3, 6 UTC, etc. Then, the regional normalization uses coincident 3-hourly GEO and CERES LW measurements within 90 min to obtain two regional simultaneous measurements per day. As with the 3-hourly SYN1deg Edition 3 product, a new set of hourbox GEO LW fluxes are estimated from linearly interpolating the 3-hourly LW fluxes. These Edition 3-like hourbox GEO LW fluxes, whether observed or interpolated, are compared to the *Terra* CERES measurements within the same hourbox. These 3-hourly GEO LW fluxes are presented in Table 3

TABLE 3. As in Table 2, but for colRH and RBA datasets with 3-hourly GEO observations.

3-h GEO dataset	Bias: GEO – CERES (%)		Std dev of regional bias (%)		RMS error (%)	
	No-norm	Norm	No-norm	Norm	No-norm	Norm
colRH	-0.66	0.02	2.81	1.24	5.55	4.46
RBA	0.43	0.11	1.46	0.80	3.48	3.19

and can be compared with the 1-hourly GEO LW fluxes in Table 2. Regional normalization removes the 3-hourly GEO LW bias as effectively as the 1-hourly GEO LW bias for both colRH and RBA. Normalization reduces both the 3-hourly or 1-hourly RBA RMS error by  $\sim 10\%$ , whereas at least a 20% reduction for both 3-hourly and 1-hourly error is realized for the colRH approach. However, introducing 1-hourly GEO reduces the normalized regional RMS error by 30% and 40% over 3-hourly GEO for the RBA\_norm and colRH\_norm approaches, respectively. Without normalization the regional RMS error is reduced by 25% and 30% for the RBA\_no-norm and colRH\_no-norm approaches, respectively, using 1-hourly GEO instead of 3-hourly GEO. Although the 1-hourly data do not change the

monthly mean regional bias, they greatly reduce the instantaneous flux bias with either method and with or without normalization.

#### d. GEO LW scene dependencies

To ensure that GEO LW dataset fluxes are not biased by viewing angle and scene conditions, the GEO LW dataset minus *Terra* CERES regional flux biases are stratified by VZA, GEO cloud fraction, PW, cloud emissivity, and lapse rate, and are plotted in Fig. 7. The colRH\_no-norm and SBA\_no-norm biases can exceed  $5 \text{ W m}^{-2}$ , whereas all of the RBA\_no-norm dataset biases are within  $5 \text{ W m}^{-2}$  over the dynamic range of the parameters. The RBA binning according to VZA, PW, and surface type is an improvement over the colRH approach. All of the RBA\_no-norm datasets are similar except for the RBA\_noMOD\_no-norm, which has the greatest bias for cloud emissivity and lapse rate. After applying regional normalization, all approach biases are mostly within  $3 \text{ W m}^{-2}$  for lapse rate and emissivity and  $1 \text{ W m}^{-2}$  for PW, cloud fraction, and VZA, and the RBA\_norm has the smallest biases overall. Normalization is essential for removing any cloud-dependent residual GEO dataset LW biases.

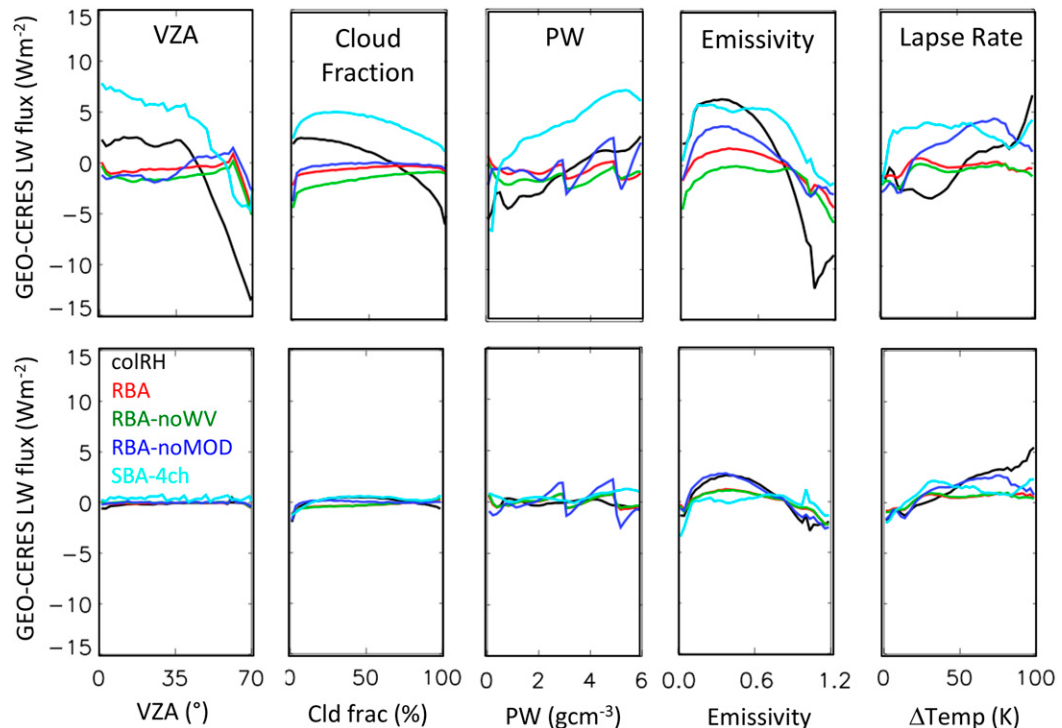


FIG. 7. The January 2010 1-h GEO LW flux dataset minus *Terra* CERES LW regional flux bias ( $\text{W m}^{-2}$ ) stratified by VZA, MODIS cloud fraction, PW, cloud emissivity, and lapse rate, and (top) without normalization and (bottom) with *Aqua* regional normalization. The datasets are from colRH (black), RBA (red), RBA without WV channel (green), RBA without MODIS channel adjustment (blue), and SBA with four-channel clouds (cyan).

## 6. Validation with GERB fluxes

The previous section validated the GEO-derived LW fluxes at the *Terra* local time only. To validate the approaches over the entire diurnal cycle, the GERB LW fluxes from January 2010 are used as truth (Harries et al. 2005). The GERB fluxes have temporal and nominal spatial resolutions of 15 min and 50 km, respectively, and cover 60°W–60°E. The GERB Edition 1 LW fluxes are 1.3% darker than CERES, but they are within the combined stated instrument calibration uncertainties. GERB may also have residual LW biases over cloudy conditions and as a function of view angle due to inadequate ADMs (Clerbaux et al. 2009). For this study, the GERB fluxes are scaled to the CERES LW fluxes to ensure the GERB and CERES flux differences do not impact the validation. For this scaling, the GERB-1 Edition 1 averaged rectified geolocated (ARG) product footprint fluxes (Dewitte et al. 2008) are averaged into the CERES equal-area grid. The coincident (within 15 min) GERB and *Terra* and *Aqua* CERES LW fluxes are then linearly regressed. The regression coefficients are shown in Eq. (5):

$$\text{LW}_{\text{CERES}} = 1.016 \times \text{LW}_{\text{GERB}} - 0.24. \quad (5)$$

The slope is very close to the 1.3% reported by Clerbaux et al. (2009), and the scatter about the regression was 3.75%. Some of this scatter can be attributed to the GERB residual ADM LW bias, which should not impact the overall GERB domain comparison. To compare specific scene conditions, a more robust GERB to CERES LW flux scaling would need to be performed.

The GERB field of view is divided into three GEO domains using the longitudes located at 37.5°W and 28°E. To minimize the time between GEO and GERB measurements, the GERB 15-min image that is closest to the GEO scan time (Table 4) is selected, ensuring that most matches occur within 15 min.

### a. With and without regional normalization

The LW fluxes from the RBA and colRH approaches are compared with the GERB LW fluxes and are shown in Fig. 8 and summarized in Tables 5 and 6. Without normalization the RBA\_no-norm shows improvement over the colRH\_no-norm for the entire GERB domain, especially in reducing all temporal-resolution RMS errors by more than 40%, except for the 1- and 3-h RMS errors, which were reduced by ~30% (Table 5). With regional normalization, the colRH\_norm, when compared with RBA\_norm, has a 10% lower monthly RMS error, similar monthly hourly RMS errors, and more than 20% greater daily, 3-, and 1-hourly RMS errors

TABLE 4. Beginning scan times for the GOEs used over the GERB domain and associated GERB scan times (min after the hour). The GOES-12 NH scan covers 60°N–20°S and the SH scan covers 20°–50°S.

Satellite	Position	GEO time	GERB time
GOES-12 NH	60°–37.5°W	45	45
GOES-12 SH	60°–37.5°W	9	0
Met-9	37.5°W–28°E	0	0
Met-7	28°–60°E	30	30

(Table 6). Regional normalization reduced the monthly and monthly 1-h RBA (colRH) RMS errors by 40% (75%) and 20% (50%), respectively, and for daily and hourly time scales by 10% (35%) and 5% (13%), respectively. Normalization is critical for both approaches but particularly for the colRH approach.

### b. Regional and instantaneous normalization

To determine the effects of the normalization method, both regional and instantaneous normalizations are applied to the RBA. Instantaneous normalization assumes that the CERES and GEO LW fluxes are associated with the same scene conditions within an hourbox. Where there is little hourly LW flux variability, the instantaneous normalization is better suited than the regional normalization, such as over the ocean off the west coast of Namibia (cf. 1-hourly flux in Fig. 8). However, over land convective regions over Brazil and Africa, regional normalization performs better. Instantaneous normalization reduces the RBA monthly RMS error by ~20% over regional normalization (Table 5). For the monthly 3-hourly and 1-hourly error, the RBA RMS errors are similar, regardless of the normalization method. However, regional normalization reduces the RBA daily, 3-, and 1-hourly RMS errors by 12%, 20%, and 17%, respectively, from the RBA with instantaneous normalization. In general, instantaneous normalization is better suited for removing monthly regional biases, whereas regional normalization increases the accuracy of higher temporal-resolution LW fluxes.

If the monthly RMS error were the only criteria for choosing the GEO LW approach, then the colRH approach with instantaneous normalization is ideal. Based on RMS errors for all other temporal resolutions, the RBA with regional normalization is preferred. Edition 4 will use the regional normalization technique since instantaneous normalization may introduce unrealistic 1-hourly GEO LW fluxes if the scene conditions within the hourbox are inconsistent. For Edition 3, Doelling et al. (2013, their Table 4, CG results) report a 0.53% monthly RMS error over the GERB domain during January 2005 using instantaneous normalization with 3-hourly GEO

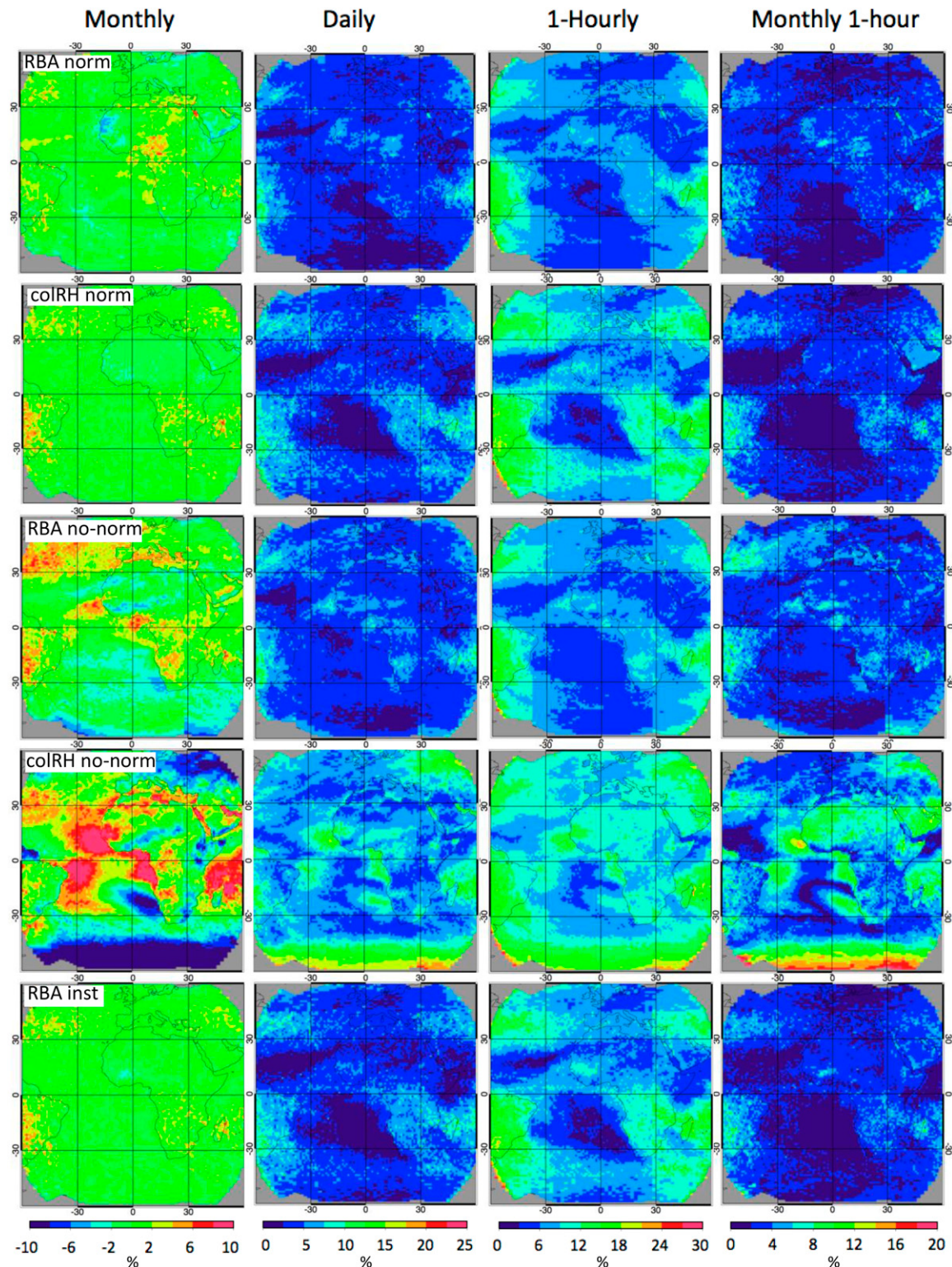


FIG. 8. The January 2010 1-h GEO LW flux dataset minus GERB LW (from left to right) monthly regional bias, daily RMS error, 1-hourly RMS error, and monthly 1-h RMS error (%). (from top to bottom) The datasets are from RBA with regional normalization, colRH with normalization, RBA without normalization, colRH without normalization, and RBA with instantaneous normalization.

TABLE 5. The RBA LW flux dataset minus GERB LW flux domain bias, monthly regional, daily, 3-hourly, 1-hourly, monthly 1-h, and monthly 3-h RMS errors using 1-h GEO observations. Regional normalization applied unless otherwise indicated.

Dataset RBA	Bias: RBA – GERB (%)	Monthly RMS (%)	Daily RMS (%)	3-h RMS (%)	1-h RMS (%)	Monthly 3-h RMS (%)	Monthly 1-h RMS (%)
Without normalization	0.20	0.99	1.72	2.62	2.95	1.26	1.39
<i>Terra + Aqua</i> normalization	0.14	0.59	1.54	2.48	2.81	0.97	1.12
<i>Terra-only</i> normalization	0.05	0.66	1.58	2.51	2.83	1.01	1.15
<i>Aqua-only</i> normalization	0.30	0.69	1.59	2.50	2.83	1.04	1.17
Instantaneous normalization	0.22	0.48	1.76	3.08	3.38	0.97	1.14

LW fluxes. The Edition 4 monthly RMS error is expected to be 0.59% (Table 5), which is slightly greater than Edition 3; however, the higher temporal-resolution RMS errors will be significantly reduced.

### c. Terra-only and Aqua-only normalization

Future CERES data products may have to rely on observations exclusively from CERES instruments on 0130 LT sun-synchronous orbits if the *Terra* instruments fail. If the GEO-derived LW fluxes were perfect, then the GEO LW fluxes normalized with *Terra* only, *Aqua* only, or *Terra + Aqua* should be identical. Doelling et al. (2013, their Table 4, CG results) found that instantaneous normalization with *Terra + Aqua* reduced the monthly and daily RMS errors by ~20% from normalization with one satellite only. Also, the *Terra*-only and *Aqua*-only GERB domain statistics were similar to each other. However, Doelling et al. (2013, their Fig. 8, CG results) showed very different monthly hourly LW fluxes depending on the satellite used for normalization. These results indicate that a discontinuity in the GEO-derived LW fluxes may be encountered when migrating to a single CERES satellite.

Both the RBA and colRH approach datasets were regionally normalized with *Aqua*-only, *Terra*-only, and *Terra + Aqua* CERES LW fluxes. The single CERES satellite results are shown in Fig. 9 and can be compared with the *Terra + Aqua* results in Fig. 8. The RBA shows more consistency among the three satellite-dependent normalizations. The monthly 1-h RMS errors of the colRH approach are clearly greater over the Sahara Desert and the Arabian Peninsula for *Terra*-only normalization than for *Aqua*-only normalization (Fig. 9).

The diurnal (monthly 1- and 3-hourly) consistency of the three satellite-dependent normalization approaches was much greater for the RBA than for the colRH approach (Tables 5 and 6). Comparisons of the satellite-dependent regional normalization of the colRH and RBA are shown in Fig. 10 for desert, maritime stratus, and convective regions, clearly illustrating the consistency of the RBA satellite-dependent normalizations. The RBA dual-satellite regional normalization mainly reduces the monthly RMS error over single-satellite normalization, whereas for the colRH approach, all temporal-resolution RMS errors were reduced. The consistency of the RBA satellite-dependent normalization implies the RBA provides more accurate LW fluxes than the colRH approach.

## 7. Conclusions

The CERES Edition 4 product reprocessing has provided the opportunity to validate the current and new GEO-derived LW flux algorithms. The Edition 4 has allowed the use of 1-hourly GEO data, improved four-channel GEO cloud retrievals, and multiple GEO IR channels to derive the LW flux. Edition 3 was based on 3-hourly GEO data and two-channel GEO cloud retrievals, and the LW flux was derived from the WIN channel and column-weighted relative humidity from an assimilated dataset. For CERES, the GEO-derived LW flux algorithm is based on the GEO IR calibration, the LW NB-to-BB algorithm, the LW flux temporal interpolation, and the normalization of the GEO-derived LW fluxes with CERES-observed fluxes. The resultant GEO LW fluxes need to be consistent across satellite

TABLE 6. As in Table 5, but for colRH.

Dataset colRH	Bias: colRH – GERB (%)	Monthly RMS (%)	Daily RMS (%)	3-h RMS (%)	1-h RMS (%)	Monthly 3-h RMS (%)	Monthly 1-h RMS (%)
Without normalization	0.21	2.19	2.94	3.86	4.14	2.41	2.49
<i>Terra + Aqua</i> normalization	0.19	0.53	1.85	3.26	3.61	1.03	1.20
<i>Terra-only</i> normalization	0.29	0.61	2.29	3.58	3.90	1.32	1.46
<i>Aqua-only</i> normalization	0.20	0.77	2.46	3.63	3.94	1.19	1.33

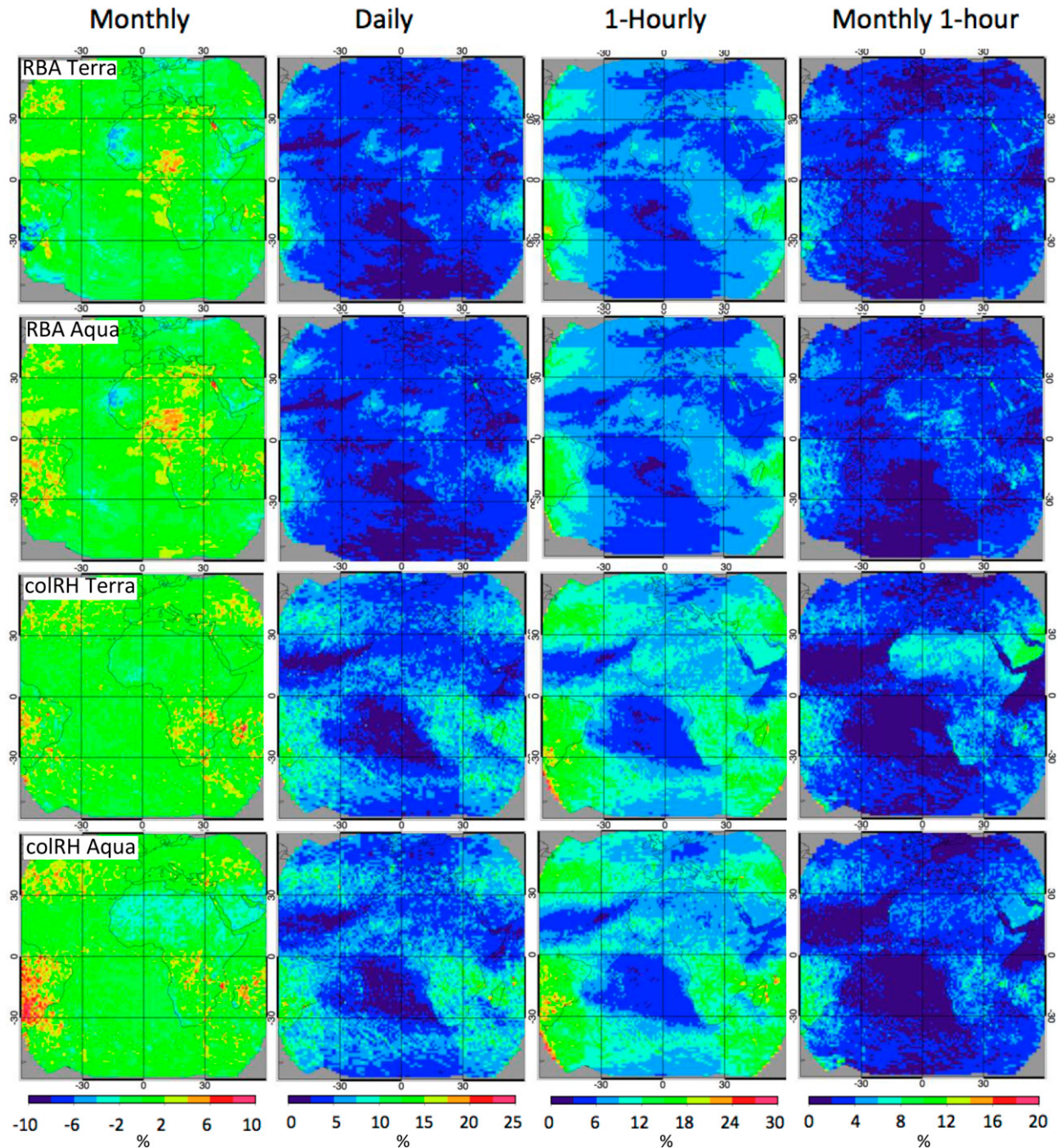


FIG. 9. The January 2010 1-h GEO LW flux dataset minus GERB LW (from left to right) monthly regional bias, daily RMS error, 1-hourly RMS error, and monthly 1-h RMS error (%). (from top to bottom) The datasets are from RBA with *Terra*-only regional normalization, RBA with *Aqua*-only regional normalization, colRH with *Terra*-only normalization, and colRH with *Aqua*-only normalization.

boundaries both spatially and temporally to prevent GEO LW artifacts being embedded in the regional LW flux natural variability.

The CERES 16-satellite GEO data record is composed of GEOs with a varying number of IR channels. Historical studies found that most of the LW flux

variability can be estimated from either a WIN or a WV channel. Fortunately, all GEO satellites during the CERES record contain both WIN and WV channels, ensuring the basis of a consistent GEO LW flux record.

Two new LW NB-to-BB flux approaches are proposed and are based on coefficients from a linear

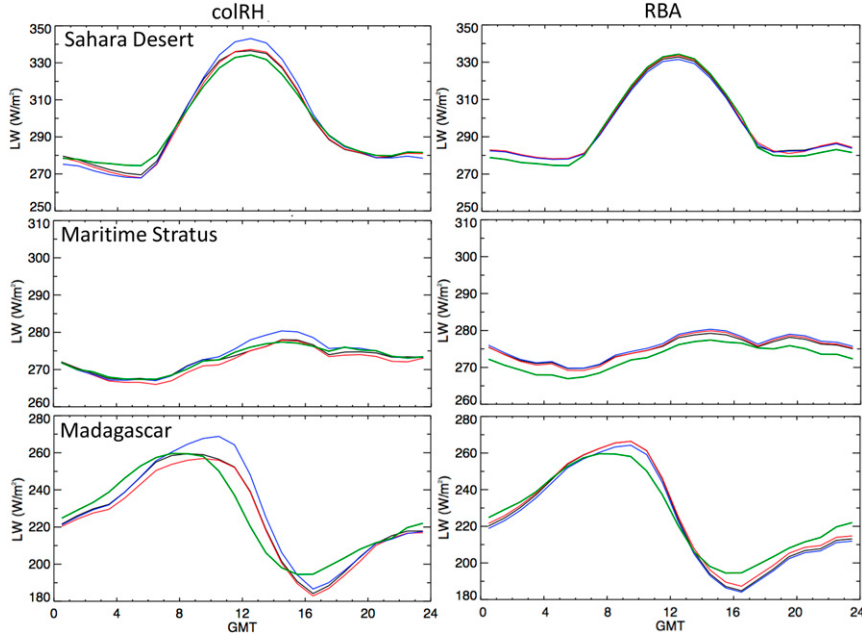


FIG. 10. The January 2010 monthly hourly GEO (left) colRH and (right) RBA datasets compared with GERB LW flux for (top row) Sahara Desert ( $15.5^{\circ}\text{N}$ ,  $20.5^{\circ}\text{E}$ ), (middle row) maritime stratus ( $20.5^{\circ}\text{S}$ ,  $10.5^{\circ}\text{E}$ ), and (bottom row) land convection ( $20.5^{\circ}\text{S}$ ,  $45.5^{\circ}\text{E}$ ) regions. Blue, red, and black lines represent the *Terra*-only, *Aqua*-only, and *Terra* + *Aqua* regionally normalized datasets, respectively. GERB is the green line used as truth for the comparison.

regression of perfectly matched CERES-observed footprint LW fluxes and MODIS radiances. The radiance-based approach (RBA) does not rely on the GEO cloud properties but uses WIN radiance, VZA, PW, and surface type bins to linearly regress the GEO WIN and WV radiances directly into LW fluxes. The scene-based approach (SBA) relies on the GEO cloud properties to further stratify by cloud parameters to linearly regress the GEO WIN and WV radiances with BB radiances. The SBA BB radiances are then converted to flux using the same CERES LW ADMs that convert the CERES radiances to fluxes. The existing Edition 3 GEO WIN channel radiance and column-weighted humidity to LW flux (colRH) approach is also evaluated.

Without normalization all approaches have significant regional LW biases, but the RBA\_no-norm has the smallest biases, especially when the GEO IR channels are intercalibrated with MODIS (Fig. 5). As intended, the regional normalization removes the regional LW flux biases from all LW NB-to-BB approaches (Fig. 5), as well as the biases dependent on VZA, PW, lapse rate, and cloud fraction and emissivity (Fig. 7). The SBA\_4ch\_norm LW flux RMS errors are found to be GEO satellite dependent (Fig. 6). The SBA\_2ch\_norm does not perform as well as the current colRH\_norm approach (Fig. 6). The SBA relies on GEO clouds that are

MODIS like, which are not achievable with the two-channel GEO retrieval algorithm.

The RBA was analyzed by comparing components and is summarized in Tables 2 and 3. Replacing the 3-hourly with 1-hourly GEO, adding the WV channel, and applying regional normalization have reduced the RMS error by 30%, 20%, and 10%, respectively, when validated with *Terra* CERES instantaneous LW fluxes, whereas the contribution from the MODIS IR adjustment was minimal. Similarly, for the colRH approach, replacing 3-hourly with 1-hourly GEO and applying regional normalization reduces the RMS error by 40% and 30%, respectively. Adding 1-hourly GEO is the most important factor in reducing the LW flux RMS error for both RBA and colRH. The RBA\_noWV\_norm and the colRH\_norm approach have regional RMS errors that are 20% and 10%, respectively, greater than the RBA\_norm. This indicates that the regional water vapor temporal variability contribution is better captured from the GEO WV channel than from an assimilated model when estimating the LW flux.

GERB comparisons in Fig. 9 show that for the *Terra*-only and *Aqua*-only datasets, the RBA regionally normalized fluxes are more consistent than those from the colRH approach, suggesting that the RBA has more accurate hourly fluxes. Instantaneous normalization is better suited in regions where the hourly time-scale

variations in LW fluxes are small, whereas regional normalization is more applicable to convective regions where the short-term LW flux variations can be dramatic (Fig. 8). To take advantage of both normalization techniques, a hybrid normalization approach may be applied for Edition 5.

The CERES Edition 4 GEO products will incorporate the 1-hourly GEO WIN and WV channel radiances adjusted to the MODIS calibration using the RBA with regional normalization to derive the GEO LW fluxes. The Edition 4 GEO LW fluxes (see Fig. 8 RBA\_norm and Table 5 Terra + Aqua normalization) are anticipated to have regional monthly LW RMS errors that are slightly greater than Edition 3 (see Fig. 8 colRH\_norm and Table 6 Terra + Aqua normalization), but with significantly reduced LW RMS errors at higher temporal resolutions. Further validation of the GEO LW fluxes is anticipated in 2016, when the entire CERES record is reprocessed as Edition 4. The new third-generation GEO satellites will offer an opportunity to reevaluate the LW approaches, by employing more IR channels to estimate the LW flux and by using improved GEO cloud retrievals that should be near MODIS like. The new GEO satellites will also offer 10-min full-disk imagery. The GEO-derived LW fluxes from using subhourly GEO sampling, which would capture more of the diurnal cycle and reduce the matching times when normalizing with CERES fluxes, should be more accurate, but they will come at a considerable data processing cost.

**Acknowledgments.** This work was funded by the NASA CERES project. The validation effort could not have been accomplished without the help of the CERES TISA team. CERES SYN1deg Edition 3 data were obtained from the NASA Langley Research Center EOSDIS Distributed Active Archive Center. GERB Edition 1 Level 2 ARG data were obtained from the GERB Ground Segment Processing System at Rutherford Appleton Laboratory. The GEOS-5 data used in this study/project were provided by the Global Modeling and Assimilation Office (GMAO) at NASA Goddard Space Flight Center.

## REFERENCES

- Cheruy, F., R. S. Kandel, and J. P. Duvel, 1991: Outgoing longwave radiation and its diurnal variation from combined ERBE and MET observations: 1. Estimating OLR from Meteosat data. *J. Geophys. Res.*, **96**, 22 611–22 622, doi:10.1029/91JD02153.
- Clerbaux, N., and Coauthors, 2009: Comparison of GERB instantaneous radiance and flux products with CERES Edition-2 data. *Remote Sens. Environ.*, **113**, 102–114, doi:10.1016/j.rse.2008.08.016.
- Dewitte, S., and N. Clerbaux, 1999: First experience with GERB ground segment processing software: Validation with CERES PFM data. *Adv. Space Res.*, **24**, 925–929, doi:10.1016/S0273-1177(99)00357-9.
- , L. Gonzalez, N. Clerbaux, A. Ipe, C. Bertrand, and B. De Paepe, 2008: The Geostationary Earth Radiation Budget edition 1 data processing algorithms. *Adv. Space Res.*, **41**, 1906–1913, doi:10.1016/j.asr.2007.07.042.
- Doelling, D. R., M. M. Khaiyer, and P. Minnis, 2003: Improved ARM-SGP TOA OLR fluxes from GOES-8 IR radiances based on CERES data. *Proc. 13th Atmospheric Radiation Measurement (ARM) Science Team Meeting*, Broomfield, CO, U.S. Dept. of Energy. [Available online at [http://www.arm.gov/publications/proceedings/conf13/extended\\_abs/doelling-dr.pdf](http://www.arm.gov/publications/proceedings/conf13/extended_abs/doelling-dr.pdf).]
- , and Coauthors, 2013: Geostationary enhanced temporal interpolation for CERES flux products. *J. Atmos. Oceanic Technol.*, **30**, 1072–1090, doi:10.1175/JTECH-D-12-00136.1.
- , A. Wu, X. Xiong, B. R. Scarino, R. Bhatt, C. O. Haney, D. Morstad, and A. Gopalan, 2015: The radiometric stability and scaling of collection 6 Terra- and Aqua-MODIS VIS, NIR, and SWIR spectral bands. *IEEE Trans. Geosci. Remote Sens.*, **53**, 4520–4535, doi:10.1109/TGRS.2015.2400928.
- Goldberg, M., and Coauthors, 2011: The Global Space-Based Inter-Calibration System. *Bull. Amer. Meteor. Soc.*, **92**, 467–475, doi:10.1175/2010BAMS2967.1.
- Gube, M., 1982: Radiation budget parameters at the top of the earth's atmosphere derived from METEOSAT data. *J. Appl. Meteor.*, **21**, 1907–1921, doi:10.1175/1520-0450(1982)021<1907:RBPATT>2.0.CO;2.
- Harries, J. E., and Coauthors, 2005: The Geostationary Earth Radiation Budget project. *Bull. Amer. Meteor. Soc.*, **86**, 945–960, doi:10.1175/BAMS-86-7-945.
- Hewison, T. J., X. Wu, F. Yu, Y. Tahara, X. Hu, D. Kim, and M. Koenig, 2013: GSICS inter-calibration of infrared channels of geostationary imagers using Metop/IASA. *IEEE Trans. Geosci. Remote Sens.*, **51**, 1160–1170, doi:10.1109/TGRS.2013.2238544.
- Lazzara, M. A., and Coauthors, 1999: The Man computer Interactive Data Access System: 25 years of interactive processing. *Bull. Amer. Meteor. Soc.*, **80**, 271–284, doi:10.1175/1520-0477(1999)080<0271:TMCIDA>2.0.CO;2.
- Lee, H.-T., A. Heidinger, A. Gruber, and R. G. Ellingson, 2004: The HIRS outgoing longwave radiation product from hybrid polar and geosynchronous satellite observations. *Adv. Space Res.*, **33**, 1120–1124, doi:10.1016/S0273-1177(03)00750-6.
- , I. Laszlo, and A. Gruber, 2008: Development of the GOES-R ABI outgoing longwave radiation product. *Fifth GOES Users' Conf.*, New Orleans, LA, Amer. Meteor. Soc., P1.8. [Available online at <https://ams.confex.com/ams/88Annual/webprogram/Paper135756.html>.]
- Li, Y., A. Wu, and X. Xiong, 2013: Evaluating calibration of MODIS thermal emissive bands using infrared atmospheric sounding interferometer measurements. *Ocean Sensing and Monitoring V*, W. W. Hou and R. A. Arnone, Eds., International Society for Optical Engineering (SPIE Proceedings, Vol. 8724), 87240X, doi:10.1117/12.2016621.
- Loeb, N. G., N. Manalo-Smith, S. Kato, W. F. Miller, S. K. Gupta, P. Minnis, and B. A. Wielicki, 2003: Angular distribution models for top-of-atmosphere radiative flux estimation from the Clouds and the Earth's Radiant Energy System instrument on the Tropical Rainfall Measuring Mission satellite. Part I: Methodology. *J. Appl. Meteor.*, **42**, 240–265, doi:10.1175/1520-0450(2003)042<0240:ADMFTO>2.0.CO;2.

- , S. Kato, K. Loukachev, and N. Manalo-Smith, 2005: Angular distribution models for top-of-atmosphere radiative flux estimation from the Clouds and the Earth's Radiant Energy System instrument on the *Terra* satellite. Part I: Methodology. *J. Atmos. Oceanic Technol.*, **22**, 338–351, doi:[10.1175/JTECH1712.1](https://doi.org/10.1175/JTECH1712.1).
- , —, W. Su, T. Wong, F. G. Rose, D. R. Doelling, J. R. Norris, and X. Huang, 2012: Advances in understanding top-of-atmosphere radiation variability from satellite observations. *Surv. Geophys.*, **33**, 359–385, doi:[10.1007/s10712-012-9175-1](https://doi.org/10.1007/s10712-012-9175-1).
- Minnis, P., D. F. Young, and E. F. Harrison, 1991: Examination of a relationship between outgoing infrared window and total longwave fluxes using satellite data. *J. Climate*, **4**, 1114–1133, doi:[10.1175/1520-0442\(1991\)004<1114:EOTRBO>2.0.CO;2](https://doi.org/10.1175/1520-0442(1991)004<1114:EOTRBO>2.0.CO;2).
- , W. L. Smith Jr., D. P. Garber, J. K. Ayers, and D. R. Doelling, 1994: Cloud properties derived from GOES-7 for spring 1994 ARM intensive observing period using version 1.0.0 of ARM Satellite Data Analysis Program. NASA Reference Publ. NASA RP-1366, 59 pp.
- , D. R. Doelling, L. Nguyen, W. F. Miller, and V. Chakrapani, 2008: Assessment of the visible channel calibrations of VIRS on TRMM and MODIS on *Aqua* and *Terra*. *J. Atmos. Oceanic Technol.*, **25**, 385–400, doi:[10.1175/2007JTECHA1021.1](https://doi.org/10.1175/2007JTECHA1021.1).
- , and Coauthors, 2011: CERES Edition-2 cloud property retrievals using TRMM VIRS and *Terra* and *Aqua* MODIS data—Part I: Algorithms. *IEEE Trans. Geosci. Remote Sens.*, **49**, 4374–4400, doi:[10.1109/TGRS.2011.2144601](https://doi.org/10.1109/TGRS.2011.2144601).
- Rienecker, M. M., and Coauthors, 2011: MERRA: NASA's Modern-Era Retrospective Analysis for Research and Applications. *J. Climate*, **24**, 3624–3648, doi:[10.1175/JCLI-D-11-00015.1](https://doi.org/10.1175/JCLI-D-11-00015.1).
- Rutan, D. A., S. Kato, D. R. Doelling, F. G. Rose, L. T. Nguyen, T. E. Caldwell, and N. G. Loeb, 2015: CERES synoptic product: Methodology and validation of surface radiant flux. *J. Atmos. Oceanic Technol.*, **32**, 1121–1143, doi:[10.1175/JTECH-D-14-00165.1](https://doi.org/10.1175/JTECH-D-14-00165.1).
- Schmetz, J., and Q. Liu, 1988: Outgoing longwave radiation and its diurnal variation at regional scales derived from *Meteosat*. *J. Geophys. Res.*, **93**, 11 192–11 204, doi:[10.1029/JD093iD09p11192](https://doi.org/10.1029/JD093iD09p11192).
- Schmit, T. J., M. M. Gunshor, W. P. Menzel, J. J. Gurka, J. Li, and A. S. Bachmeier, 2005: Introducing the next-generation Advanced Baseline Imager on *GOES-R*. *Bull. Amer. Meteor. Soc.*, **86**, 1079–1096, doi:[10.1175/BAMS-86-8-1079](https://doi.org/10.1175/BAMS-86-8-1079).
- Singh, R., P. K. Thapliyal, C. M. Kishtawal, P. K. Pal, and P. C. Joshi, 2007: A new technique for estimating outgoing longwave radiation using infrared window and water vapor radiances from Kalpana very high resolution radiometer. *Geophys. Res. Lett.*, **34**, L23815, doi:[10.1029/2007GL031715](https://doi.org/10.1029/2007GL031715).
- Sohn, B. J., H.-S. Park, H.-J. Han, and M.-H. Ahn, 2008: Evaluating the calibration of *MTSAT-IR* infrared channels using collocated *Terra* MODIS measurements. *Int. J. Remote Sens.*, **29**, 3033–3042, doi:[10.1080/01431160701408394](https://doi.org/10.1080/01431160701408394).
- , B.-R. Kim, and S.-S. Lee, 2010: Possible shift of spectral response function of the MODIS 6.8  $\mu\text{m}$  water vapor channel causing a cold bias of 2–3 K. *Atmos. Meas. Tech.*, **3**, 1667–1672, doi:[10.5194/amt-3-1667-2010](https://doi.org/10.5194/amt-3-1667-2010).
- Sun, J., S. Madhavan, B. N. Wenny, and X. Xiong, 2011: Terra MODIS band 27 electronic crosstalk: Cause, impact and mitigation. *Sensors, Systems, and Next-Generation Satellites XV*, R. Meynart, S. P. Neek, and H. Shimoda, Eds., International Society for Optical Engineering (SPIE Proceedings, Vol. 8176), 81760Z, doi:[10.1117/12.897754](https://doi.org/10.1117/12.897754).
- Taylor, P. C., and N. G. Loeb, 2013: Impact of sun-synchronous diurnal sampling on tropical TOA flux interannual variability and trends. *J. Climate*, **26**, 2184–2191, doi:[10.1175/JCLI-D-12-00416.1](https://doi.org/10.1175/JCLI-D-12-00416.1).
- Viollier, M., R. Kandel, and P. Raberanto, 2004: Combination of ScaRaB-2 and CERES with *Meteosat-5* to remove time sampling bias and improve radiation budget estimations in the INDOEX region. *J. Geophys. Res.*, **109**, D05105, doi:[10.1029/2003JD003947](https://doi.org/10.1029/2003JD003947).
- Wielicki, B. A., B. R. Barkstrom, E. F. Harrison, R. B. Lee III, G. L. Smith, and J. E. Cooper, 1996: Clouds and the Earth's Radiant Energy System (CERES): An Earth Observing System experiment. *Bull. Amer. Meteor. Soc.*, **77**, 853–868, doi:[10.1175/1520-0477\(1996\)077<0853:CATERE>2.0.CO;2](https://doi.org/10.1175/1520-0477(1996)077<0853:CATERE>2.0.CO;2).
- , and Coauthors, 2013: Achieving climate change absolute accuracy in orbit. *Bull. Amer. Meteor. Soc.*, **94**, 1519–1539, doi:[10.1175/BAMS-D-12-00149.1](https://doi.org/10.1175/BAMS-D-12-00149.1).
- Young, D. F., P. Minnis, D. R. Doelling, G. G. Gibson, and T. Wong, 1998: Temporal interpolation methods for the Clouds and the Earth's Radiant Energy System (CERES) experiment. *J. Appl. Meteor.*, **37**, 572–590, doi:[10.1175/1520-0450\(1998\)037<0572:TIMFTC>2.0.CO;2](https://doi.org/10.1175/1520-0450(1998)037<0572:TIMFTC>2.0.CO;2).